Journal of Power Sources 273 (2015) 340–350

Contents lists available at ScienceDirect

Journal of Power Sources

journal homepage: www.elsevier.com/locate/jpowsour

Enhancing the efficiency of direct carbon fuel cells by bubbling Ar gas in carbon/carbonate slurry

Hirotatsu Watanabe*, Tomoaki Furuyama, Ken Okazaki

Department of Mechanical and Control Engineering, Graduate School of Science and Engineering, Tokyo Institute of Technology, I6-7, 2-12-1, Ookayama, Meguro-ku, Tokyo 152-8552 Japan

HIGHLIGHTS

- DCFC developed here uses a porous alumina tube to contain carbon/carbonate slurry.
- Bubbling in carbon/carbonate slurry impact is dictated by the C/O^{2-} ratio.
- Bubbling inhibits partial electrochemical oxidation when the C/O^{2-} ratio is low.
- Bubbling increases total efficiency from 52 % to 64 % for $W_{C/carbonate} = 1.0$ wt%.

ARTICLE INFO

Article history:
Received 12 August 2014
Received in revised form
9 September 2014
Accepted 11 September 2014
Available online 19 September 2014

Keywords:
DCFC
Coulombic efficiency
Bubbling
Molten carbonate
Electrochemical oxidation

ABSTRACT

This study aims to enhance the direct carbon fuel cell (DCFC) efficiency by bubbling Ar gas in a carbon/carbonate slurry. The current discharge curve and CO and CO_2 production rates were measured during discharge at 20 mA cm^{-2}. When carbon content in carbonates ($W_{C/carbonate}$) was 1.0 wt%, Ar bubbling decreased the CO/CO_2 production ratio from 0.16 to 0.051, and increased the CO_2 production rate, which approached the theoretical value for complete electrochemical oxidation of carbon. Moreover, bubbling increased the cell voltage by about 0.1 V at steady state. At $W_{C/carbonate} = 3.0$ wt%, the CO/CO_2 production ratio without bubbling increased significantly to 8.5, indicating that partial electrochemical oxidation became dominant. The C/O^{2-} ratio is key for explaining the electrochemical oxidation of the carbon. When the C/O^{2-} ratio was low, such as at $W_{C/carbonate} = 1.0$ wt%, complete electrochemical oxidation became dominant, and bubbling enhanced the complete electrochemical oxidation. When the C/O^{2-} ratio was high, such as at $W_{C/carbonate} = 3.0$ wt%, partial electrochemical oxidation became dominant, and bubbling did not inhibit it. For $W_{C/carbonate} = 1.0$ wt%, bubbling increased both coulombic and voltage efficiencies, resulting in an increase in total efficiency from 52% to 64%.

1. Introduction

Fuel cells are able to efficiently convert the chemical energy from fuels into electrical energy. However, conventional fuel cells like proton-exchange fuel cells (PEFCs) and solid oxide fuel cells (SOFCs) use gaseous fuels. Conversion of energy from solid carbon fuels such as coal or biomass chars in these cells requires gasification. In contrast, direct carbon fuel cells (DCFCs) convert the chemical energy in carbon directly into electricity, without the need for gasification. The solid carbon fuels used in DCFCs can be produced from sources such as coal, natural gas, and biomass. Fine carbon particles are electrochemically oxidized at high temperatures ($C + O_2 \rightarrow CO_2$).

Although variety of DCFC designs have been tested, and some articles related to DCFCs have recently been published [1–3], this technology is still in the preliminary stage of development [1]. There have been various attempts to convert carbon materials directly into electricity in DCFCs using electrolytes, such as molten carbonates [4–7], molten hydroxides [8], and YSZ-based solid electrolytes [9,10]. The use of molten carbonate has a number of advantages: it has good long-term stability in CO_2, can catalyze carbon oxidation, and has a high ionic conductivity [1]. When carbon particles such as pulverized chars are used in DCFCs, carbon/carbonate slurry is an appropriate fuel for improving contact with metal current collector or anode.

* Corresponding author. Tel./fax: +81 3 5734 2179.
E-mail address: watanabe.h.ak@m.titech.ac.jp (H. Watanabe).

http://dx.doi.org/10.1016/j.jpowsour.2014.09.079
0378-7753/

The anode (R1), cathode (R2), and overall reaction (R3) in this system are expressed as follows:

$$C + 2CO_3^{2-} \rightarrow 3CO_2 + 4\,e^- \quad (R1)$$

$$O_2 + 2\,CO_2 + 4\,e^- \rightarrow 2\,CO_3^{2-} \quad (R2)$$

$$C + O_2 \rightarrow CO_2 \quad (R3)$$

The desired reaction is complete oxidation, which releases four electrons per carbon, as given by R1. However, several studies have shown a possible formation of CO at the anode compartment from R4, R5, or even from the Boudouard reaction (R6) [4,6,11–14].

$$C + CO_3^{2-} \rightarrow CO + CO_2 + 2e^- \quad (R4)$$

$$C + 1/2CO_3^{2-} \rightarrow 3/2CO + e^- \quad (R5)$$

$$C + CO_2 \rightarrow 2CO \quad (R6)$$

Two electrons are released per carbon atom in R4, whereas only one electron is released per carbon atom in R5. However, this aspect remains speculative because gas analysis was not always provided or performed in the relevant research studies [11].

The total electrochemical efficiency of a DCFC is determined by its voltage efficiency (the ratio of cell voltage to theoretical voltage) and coulombic efficiency (electron yield (n) per carbon atom, divided by 4) [15]. Cooper and Selman derived a coulombic efficiency formula in DCFC from two reactions (R1 and R4) [16], and a recent study has employed coulombic efficiency data to evaluate DCFC performance [17]; however, little effort has been made to enhance coulombic efficiency by inhibiting partial electrochemical oxidations (R4 and R5).

This study aims to enhance DCFC efficiency by bubbling an inert gas in a carbon/carbonate slurry. Inert gas bubbling can be easily applied to stir highly corrosive molten carbonates. The current discharge curve and CO and CO_2 production rates were measured, and partial electrochemical oxidations were studied.

2. Experimental section

2.1. Carbon characterizations

Commercial activated carbon (activated charcoal, Kantokagaku) was used in this study. Elemental composition of activated carbon was determined using CHN elemental analyzer (Micro corder JM10, J-Science Lab Co. Ltd.) and sulfur analyzer (HSU-20, J-Science Lab Co. Ltd.). Characterization of the activated carbon was performed by X-ray diffraction (X'Pert MPD, Philips) with Cu Kα radiation at 40 kV and 30 mA. The size distribution of activated carbon was measured by laser diffraction (LMS-2000e, Seishin Enterprise Co., Ltd.).

2.2. DCFC experiments

Fig. 1 shows a schematic diagram of a DCFC with a molten carbonate electrolyte, which was developed in our laboratory. In this study, the working electrode (WE), counter electrode (CE), and reference electrode (RE) were made from gold sheet. The area in contact with the carbon was 1.0 cm^2. The RE and CE were in alumina tubes, and the WE was in a porous alumina tube (for separation of carbon particles, as described later). Each gold sheet was spot welded to the gold wire and extended to the other end of the tube to provide a connection to the potentiostat/galvanostat (HAL-3001, Hokuto Denko) for cell parameter measurements. On the basis of cell measurements, current density was set at 20 mA cm^{-2} during discharge. Carbonate easily corrodes quartz; therefore, a high purity alumina crucible was used as a holder for carbonate. In order to keep the entire cell in a gastight environment, the alumina crucible was placed at the bottom of the quartz reactor with O-rings and silicone plugs. The gas feed tubes for the counter electrode (CE) and the reference electrode (RE), and the porous tube for the working electrode (WE) were made from high purity alumina, and these were supported by silicone plugs attached to the top of the quartz reactor as a gas seal. The alumina crucible contained 243 g of dry ternary carbonate powder (Li_2CO_3:Na_2CO_3:K_2CO_3 = 1:4:4 (weight ratio)) without carbon, and the mixed carbon/carbonate powder was contained in the porous alumina tube having an average pore diameter of 95.6 nm. Therefore, carbon particles larger than this size did not pass through the porous alumina tube. This allowed contact between the molten carbonate electrolyte and WE, CE, and RE. In the porous alumina tube, the mixed carbon/carbonate powder consisted of 11.3 g of dry ternary carbonate powder (Li_2CO_3:Na_2CO_3:K_2CO_3 = 1:4:4 (weight ratio)) and 0.113 g or 0.339 g of activated carbon (i.e., 1.0 wt% or 3.0 wt% of the carbon fuel in the carbonates, defined as $W_{C/carbonate}$). Although the single carbonate has relatively high melting point: Li_2CO_3 (999 K), Na_2CO_3 (1131 K), and K_2CO_3 (1172 K), the eutectic carbonate has much lower melting point; therefore, ternary eutectic carbonate has been generally used in the DCFC with a molten carbonate electrolyte [7].

After the fuel cell was assembled and sealed to be gastight, the reactor was heated using an electric furnace to 1073 K. Ar (100 ml min^{-1}) was introduced into the WE compartment during heating. After the carbonate powder melted, alumina tubes with CE and RE were inserted into the molten carbonates in the alumina crucible. Then, O_2 (50 ml min^{-1}) and CO_2 (100 ml min^{-1}) gases were introduced. The DCFC developed here was similar to that developed in previous studies [4,6,12,14]; but, there were some differences. In the DCFCs used in previous studies, carbon/carbonate slurry contacted the WE that was contained in an alumina crucible, and pure carbonates electrolyte contacted the CE and RE that was contained in an alumina tube with holes. In contrast, here the carbon/carbonate slurry was contained in the porous alumina tube, and pure carbonates were contained in the alumina crucible. The positions of the carbon/carbonate slurry and the carbonate in the DCFCs in this study were opposite to the positions in DCFCs in previous studies [4,6,12,14]. Containing the carbon/carbonate slurry in the porous alumina tube is advantageous because the slurry is easily exchanged by using new porous alumina tube with the slurry when ash accumulates over time with the use of coal chars. In this study, activated carbon was used as fuel. However, coal chars were used as well. Build-up of ash in the molten carbonate electrolyte is one of the main barriers in DCFC development [5]. The DCFC developed in this study is of a cartridge type, and the cell stack is packaged by using several anode compartments consisting of porous alumina tubes and carbon/carbonate slurry.

This DCFC comprised WE, CE, RE, and reactor compartments. Herein, a reactor compartment is a space in the quartz reactor, excluding the WE, CE, and RE compartments. Anode off gases from WE were able to pass through the porous alumina tube, and diffuse to the reactor compartments. Therefore, after reaching steady state, CO_2 and CO concentrations in anode-off gases from WE and reactor compartments ($X_{CO2,WE}$, $X_{CO2,reactor}$, $X_{CO,WE}$, $X_{CO,reactor}$) were measured with a flame ionization detector (FID) equipped with a Porapack-Q column and methanizer. Outlet gas flow rates (Q_{WE}, and $Q_{reactor}$) were also measured, using a wet gas meter (W-NK-1, Shinagawa Co., Ltd).

CO_2 and CO flow rates (Q_{CO2} and Q_{CO}) are given as follows:

$$Q_{CO_2} = \sum_i \left(X_{CO_2,i} Q_i \big|_{\text{no discharge}} \right) \quad \left(i = \text{WE, reactor compartment} \right) \quad (1)$$

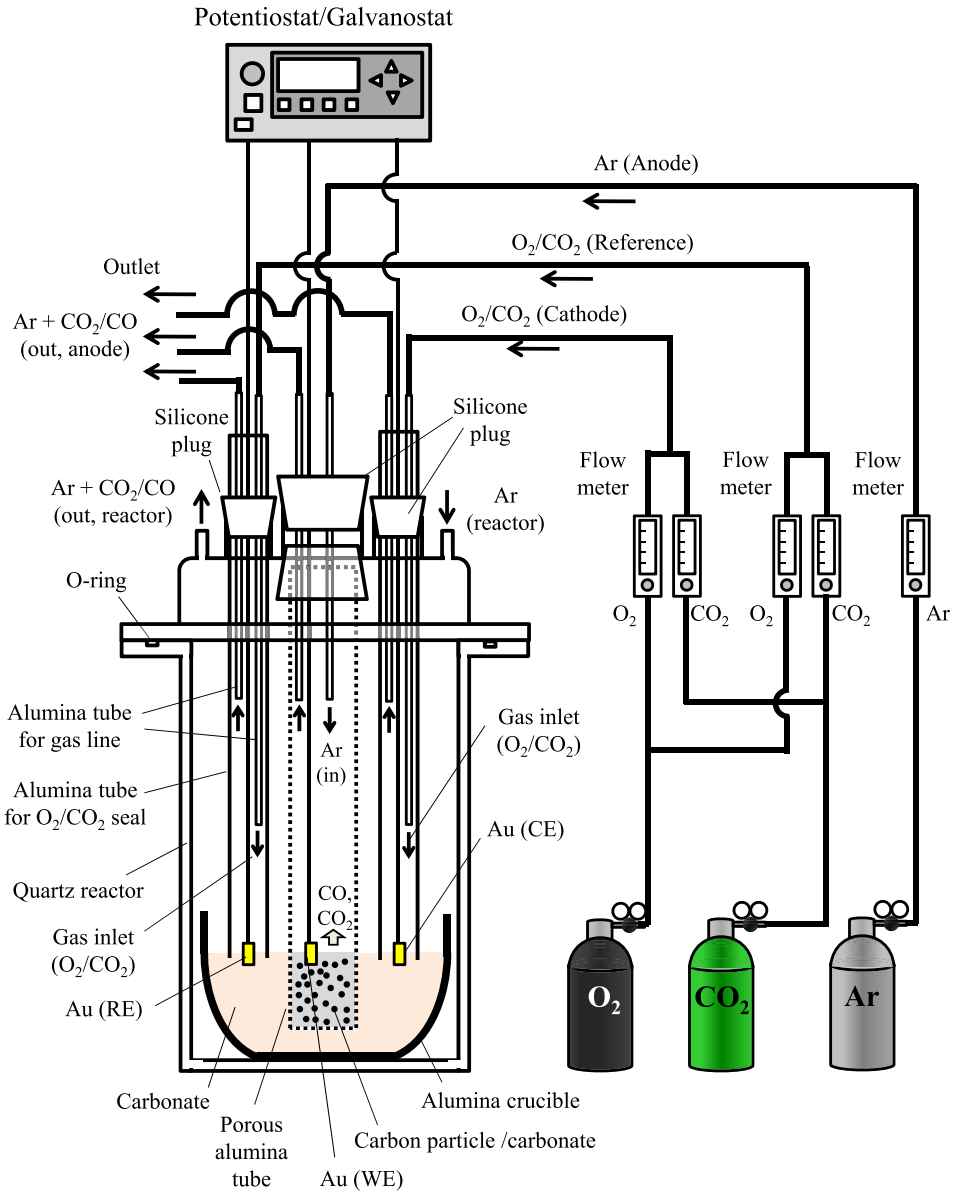

Fig. 1. Schematic diagram of DCFC with a molten carbonate electrolyte using porous alumina tube in anode compartment.

$$Q_{CO} = \sum_i \left(X_{CO,i} Q_i |_{\text{no discharge}} \right) \quad \left(i = \text{WE, reactor compartment} \right) \tag{2}$$

CO_2 and CO production rates ($Q_{CO2,product}$ and $Q_{CO,product}$) are determined by the sum of the differences between CO_2 and CO flow rates during discharge (at 20 mA cm^{-2}) and those at the OCV (open circuit voltage) condition, given as:

$$Q_{CO_2,product} = \sum_i \left(X_{CO_2,i} Q_i |_{\text{discharge}} - X_{CO_2,i} Q_i |_{\text{no discharge}} \right) \quad (i = \text{WE, reactor compartment}) \tag{3}$$

$$Q_{CO,product} = \sum_i \left(X_{CO,i} Q_i |_{\text{discharge}} - X_{CO,i} Q_i |_{\text{no discharge}} \right) \quad (i = \text{WE, reactor compartment}) \tag{4}$$

The CO_2 production rate at the time discharge is processed through R1 and at constant is calculated as follows:

$$Q_{CO_2,product} = \frac{3 I V_m}{4F} \tag{5}$$

where F is the Faraday constant (96,450 C mol^{-1}), V_m is the molar volume of CO_2 at standard temperature and pressure, and I is the constant current flow. Unit of Ampere corresponds to coulomb per second (C s^{-1}). The CO_2 production rate is 0.209 ml min^{-1} when I is 20 mA. Anode-off gases were measured before discharge, confirming that O_2 concentration was negligible in the anode and reactor compartments.

2.3. Ar bubbling in anode compartment

Fig. 2 shows a schematic diagram of the anode compartment with (a) and without (b) bubbling. Ar gas for bubbling was released from two holes in a gas line tube. The diameters of the holes were 2 mm. When the carbon/carbonate slurry was used as fuel in DCFCs, fuel stirring played an important role in determining the electrochemical performance [4,6]. In this study, fuel was stirred using Ar

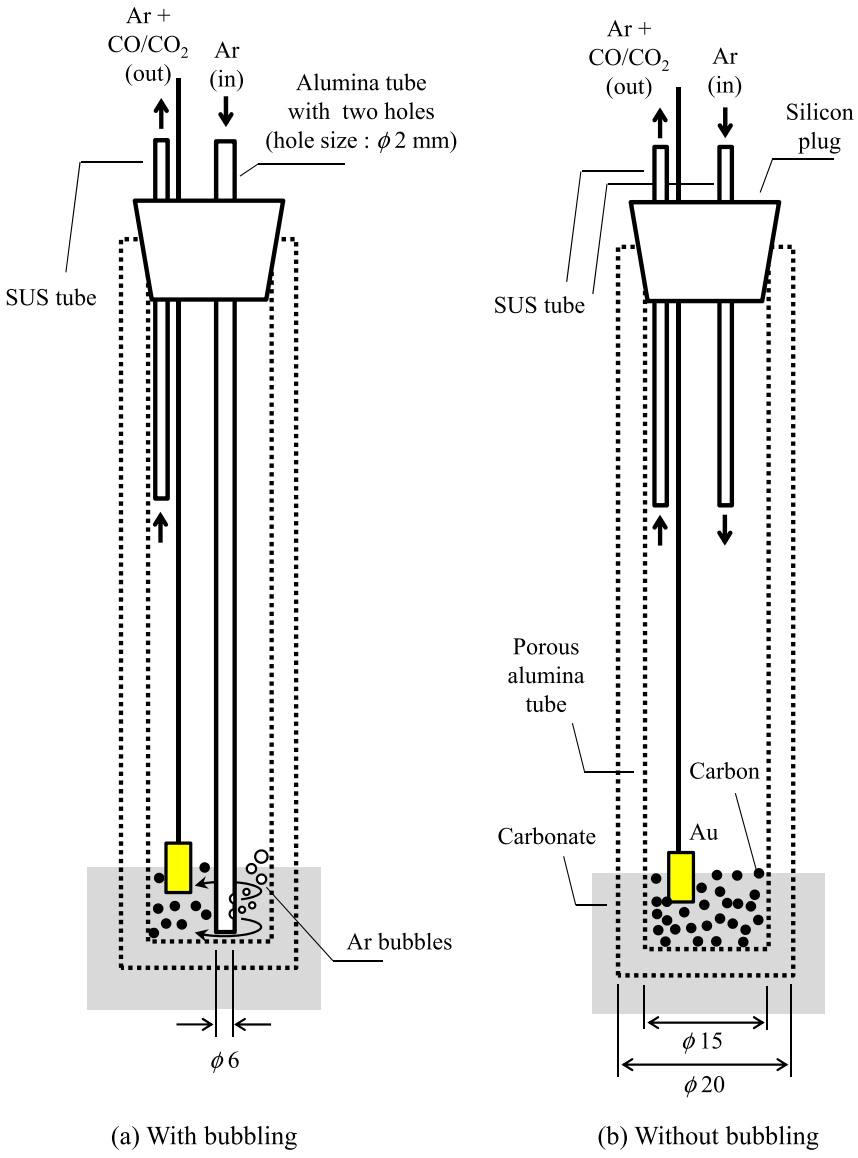

Fig. 2. Schematic diagram of anode compartment with or without bubbling.

gas bubbling with a flow rate of 50 ml min^{-1}. For stirring molten carbonates, high purity aluminum or other materials resistant to highly corrosive molten carbonates are required. In contrast, inert gas bubbling is easier to use with molten carbonates. Bubbling is supposed to stir the carbon/carbonate slurry, and provide carbons and ions to the anode surface. Unlike mechanical stirring, bubbling is also expected to immediately remove gases (CO_2 and CO) resulting from the electrochemical reaction.

3. Results and discussion

3.1. Carbon characterizations

Table 1 shows an elemental analysis (dry-base) and the ash content of samples.

Fig. 3 shows the XRD pattern of the activated carbon. Graphite carbon was also analyzed for reference, and an intense peak corresponding to the (002) graphitic basal plane reflection was observed at $2\theta = 26.5$. These peaks are relatively low, indicating disordered structure than graphite carbon, which is consistent with previous studies [6,14]. The average size of carbon crystalline was calculated from the Debye–Scherer equation [6]. Constants in the Debye–Scherer equation were 0.9 for L_c (the layer dimension perpendicular to the basal plane) and 1.84 for L_a (the layer dimension parallel to the basal plane). The crystalline parameters, d_{002} (interplanar distance), L_c, and L_a are shown in Table 2. The relationship between carbon properties and OCV in the DCFC will be discussed later.

Fig. 4 shows the size distribution of activated carbon. The average diameter of activated carbon was 22.4 μm. Thus, the activated carbon did not pass through the porous alumina tube used in the DCFC cell.

3.2. Anode off gas characteristics

Fig. 5 shows measured CO_2 and CO flow rates without bubbling at the OCV condition ($I_d = 0$ mA cm^{-2}) and $I_d = 20$ mA cm^{-2}, and CO

Table 1
Elemental analysis of the activated chars [wt%, dry].

C	H	N	S	O (diff)	Ash
92.3	0.17	3.04	0.10	4.39	0.8

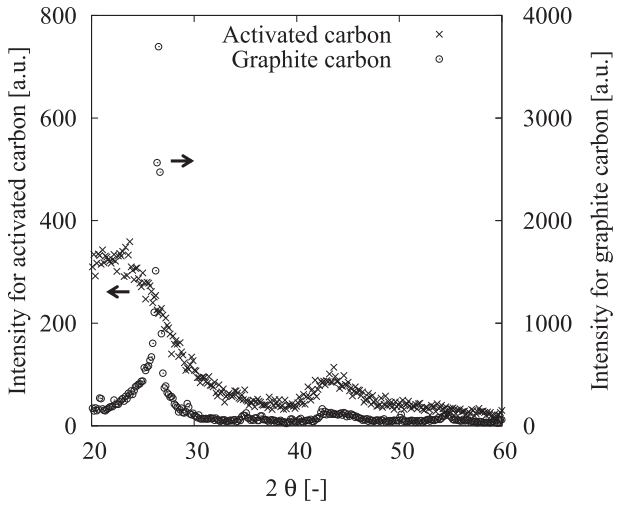

Fig. 3. XRD patterns of activated and graphite carbon.

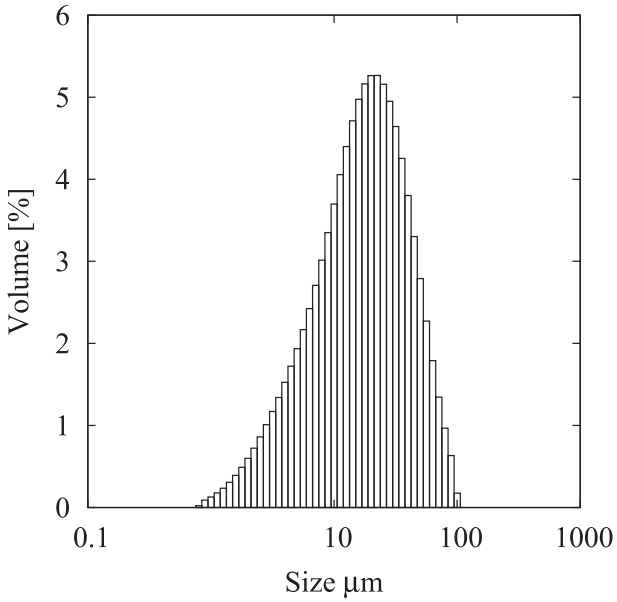

Fig. 4. Size distribution of activated carbon.

estimation at $W_{C/carbonate} = 1.0$ wt%. Some carbonate was contained in the alumina crucible; therefore, CO_2 was formed at the OCV condition as a consequence of the carbonate decompositions given by R7 [18–20];

$$M_2CO_3 \rightarrow M_2O + CO_2 \quad (R7)$$

where M is K, Na or Li. CO_2 formation at the OCV condition also indicates M_2O formation. Especially, the single Li_2CO_3 starts to decompose at lower temperature than the reaction temperature of 1073 K [20]. Li_2O is an important species to achieve a higher OCV in DCFCs as described later. CO is also produced at the OCV condition. In addition to R6, CO forms through carbothermic reactions given as R8 and R9 [18–20].

$$M_2CO_3 + C \rightarrow M_2O + 2CO \quad (R8)$$

$$M_2O + C \rightarrow 2M + CO \quad (R9)$$

CO_2 and CO flow rates increased at $I_d = 20$ mA cm^{-2}. The increase in CO_2 comes from electrochemical oxidations given as R1 and R4. There are two possible oxidation reactions resulting in the CO increase during discharge. One is the Boudouard reaction, and the other is partial electrochemical oxidation. An increase in CO_2 during discharge may increase the rate of the Boudouard reaction. If this is the case, then the rate of increase of CO is the same as that of CO_2 because the reaction rate of R6 has a linear relationship with CO_2 concentration. In addition to this, here, CO is assumed to form through R6 at OCV condition. CO flow rate estimated from these assumptions is described as "OCV + R6". However, the measured CO flow rate at $I = 20$ mA was about 70% higher than the estimated value, suggesting that the dominant reaction in CO formation during discharge is not the Boudouard reaction but partial electrochemical oxidation.

Fig. 6 shows measured CO_2 and CO flow rates without bubbling in the OCV condition ($I_d = 0$ mA cm^{-2}) and $I_d = 20$ mA cm^{-2}, and CO estimation at $W_{C/carbonate} = 3.0$ wt%. In the OCV condition, CO concentration at $W_{C/carbonate} = 3.0$ wt% was almost three times that at $W_{C/carbonate} = 1.0$ wt%. This indicates that CO is produced through R6, R8, and R9, because these reaction rates have linear relations with carbon content in carbonates. At $W_{C/carbonate} = 3.0$ wt%, the discharge process does not increase CO_2 flow rate, but it significantly increases CO flow rate. This is clear evidence that partial electrochemical oxidation plays an important role during discharge at higher carbon content, as discussed in detail later in this study.

Table 2
Crystalline parameters of activated chars.

d_{002} [nm]	L_c [nm]	L_a [nm]
0.376	0.987	3.22

3.3. Effect of bubbling on current discharge curves and anode off gases

Fig. 7 shows the effect of bubbling on constant current discharge curves at $W_{C/carbonate} = 1.0$ wt%. Voltage at $t = 0$ min corresponds to the OCV condition. At $W_{C/carbonate} = 1.0$ wt%, OCVs with and without bubbling are 1.15 V and 1.27 V, respectively (see Fig. 7(a)). The standard potential of R1 (C (graphite) + $O_2 \rightarrow CO_2$) is 1.026 V as evaluated from the Gibbs energy change at 1073 K [21]; however, experimental OCV is generally higher than the standard potential of graphite carbon as a consequence of carbon properties and gas composition [5,22,23]. As shown in Fig. 3, the activated carbon has disordered structure. The highly pore crystallized, lattice disordered carbons are more reactive than highly oriented pyrolytic graphite, resulting in higher OCVs [22]. However, even if these factors are considered; 1.27 V is significantly higher than the standard potential. In several studies, OCV values of 1.2–1.5 V were reported. Such values are significantly higher than the thermodynamically expected value ($E_0 = 1.026$ V at 1073 K) [24–26]. These high OCV values suggest the intervening role of CO and/or the alkali ions in the molten carbonate participating in the anode reaction [25,26]. When CO participation is considered as R10, the thermodynamically expected value is still lower. However, if Li^+ is considered as the counter cation, net cell reactions are described as R11 and R12, and OCVs are higher than 1.026 V:

$$CO + 1/2O_2 \rightarrow CO_2 \ (E^0 = 0.98 \text{ V at } 1073 \text{ K}) \quad (R10)$$

$$C\,(s) + O_2\,(g) + Li_2O\,(cr) \rightarrow Li_2CO_3\,(cr) \ (E^0 = 1.18 \text{ V at } 1073 \text{ K}) \quad (R11)$$

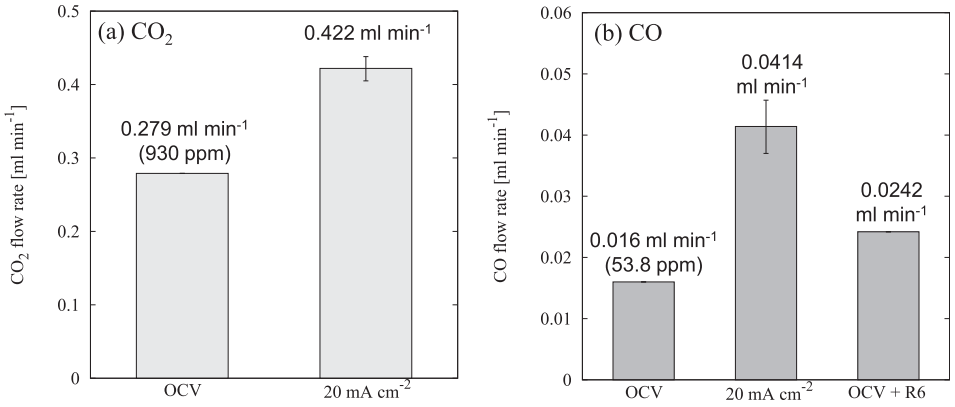

Fig. 5. Measured CO_2 and CO flow rate without anode bubbling at OCV (I = 0 mA cm^{-2}), I = 20 mA cm^{-2}, and estimation (OCV + R6) ($W_{C/carbonate}$ = 1.0 wt%).

$$CO\ (g) + 1/2O_2\ (g) + Li_2O\ (cr) \rightarrow Li_2CO_3\ (cr)$$
$$(E^0 = 1.30\ V \text{ at } 1073\ K) \quad (R12)$$

Details of R11 and R12 are described in Refs. [25,26]. The literature suggests that R12 provides an acceptable explanation of high OCV of 1.3 V [24–26]. As previously described, CO is formed by R6, R8, and R9, and Li_2O is formed by R7 and R8. This also explains why Ar bubbling decreases OCV. Ar bubbling is supposed to remove gases from carbon/carbonates slurry immediately; therefore, Ar bubbling decreases OCV to 1.1–1.2 V by removing CO before it consumes through R12. Meanwhile, Ar bubbling improves the current discharge curve at steady state. At the beginning of the discharge process, the cell voltage rapidly decreases, and then becomes almost constant.

To calculate the theoretical CO flow rate through R12, it is assumed that R12 consists of following anode reaction (R13).

$$CO + O^{2-} + Li_2O \rightarrow Li_2CO_3 + 2e^- \quad (R13)$$

Based on R13, the theoretical CO flow rate necessary for 20 mA cm^{-2} discharge is 0.139 ml min^{-1}. However, CO flow rate is 0.016 ml min^{-1} at the OCV condition, which is much lower than the theoretical value. Thus, cell voltage decreases rapidly when bubbling is not used. Bubbling increases the cell voltage at approximately 3–5 min in current discharge curves, and cell voltage obtained with bubbling is higher than that without bubbling by approximately 0.1 V at 20 min. This is because bubbling is supposed to stir the fuel/carbonate slurry, and as a result it provides both carbon and ions to reaction sites. In fact, the voltage reduction results from diffusion polarization.

Fig. 8 shows the effect of bubbling on constant current discharge curves at $W_{C/carbonate}$ = 3.0 wt%. At $W_{C/carbonate}$ = 3.0 wt%, the OCV difference between with and without bubbling is less than 3%. It could be due to an experimental error. Finding here is that bubbling does not influence the current discharge curve in contrast to that at $W_{C/carbonate}$ = 1.0 wt%, and the OCV obtained is 1.3–1.4 V. This is because CO concentration at $W_{C/carbonate}$ = 3.0 wt% is about three times higher than that at $W_{C/carbonate}$ = 1.0 wt% at the OCV condition. Although Ar bubbling promoted the removal of gases from the carbon/carbonates slurry, complete removal of CO is beyond the capacity of Ar bubbling. Moreover, CO concentration increases significantly because of partial electrochemical oxidation during discharge, and it is higher than the 0.139 ml min^{-1} that is necessary for a 20 mA cm^{-2} discharge. Therefore, R12 plays an important role in discharge at $W_{C/carbonate}$ = 3.0 wt%, leading to higher cell voltage than at $W_{C/carbonate}$ = 1.0 wt%. Although it is difficult to determine the minimum CO concentration that is needed to have an effect on the OCV, the findings described herein provide acceptable explanations for the insignificant effect of Ar bubbling on the current discharge curve at $W_{C/carbonate}$ = 3.0 wt%.

Fig. 9 shows the effect of bubbling on measured CO_2 and CO production rates during discharge at $W_{C/carbonate}$ = 1.0 wt%. Ar bubbling decreases the CO/CO_2 production ratio from 0.16 to 0.051, and increases the CO_2 production rate, which approached the theoretical value (=0.209 ml min^{-1}).

Fig. 10 shows the effect of bubbling on measured CO_2 and CO production rates during discharge at $W_{C/carbonate}$ = 3.0 wt%. The CO/CO_2 ratios with and without bubbling are 8.5 and 9.0, respectively. In contrast to the result at $W_{C/carbonate}$ = 1.0 wt%, bubbling increases the CO production rate at $W_{C/carbonate}$ = 3.0 wt%, because it removes

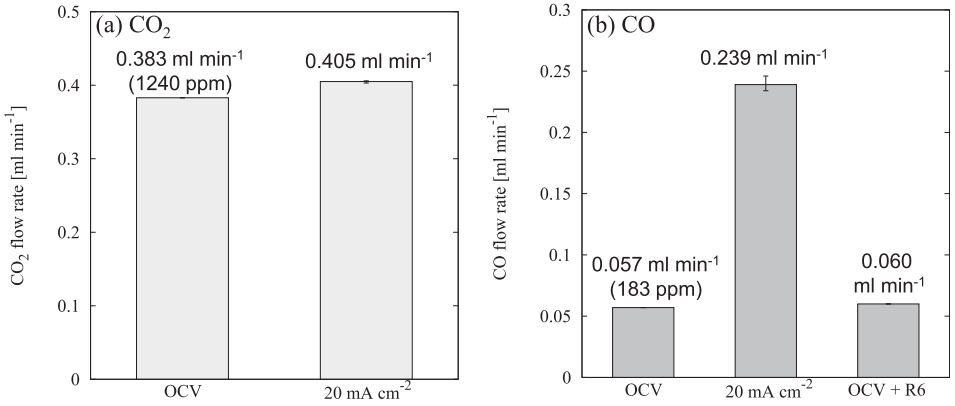

Fig. 6. Measured CO_2 and CO flow rate without anode bubbling at OCV, 20 mA cm^{-2} and estimation (OCV + R6) ($W_{C/carbonate}$ = 3.0 wt%).

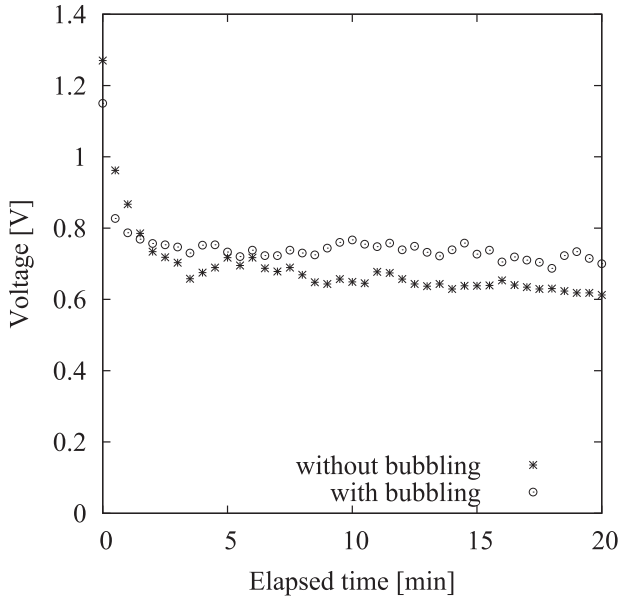

Fig. 7. Effect of bubbling on constant current discharge curves at 20 mA cm^{-2} and $W_{C/carbonate}$ = 1.0 wt%.

CO from the slurry before it is consumed through R12. The products of R12 are not gases; thus, the CO production rate is increased by inhibiting R12, as discussed below.

3.4. Electrochemical oxidation of carbon, and coulombic efficiency

Elemental reaction pathways for complete and partial electrochemical oxidations of carbon are illustrated in Fig. 11, referring previous studies [3,5,15,27,28]. The reaction is initiated by the dissociation of carbonate to form O^{2-} through R14 [3,5]. Carbon and carbonate also react, producing CO and O^{2-} through R15 [27,28].

$$CO_3^{2-} \rightarrow CO_2 + O^{2-} \quad \text{(R14)}$$

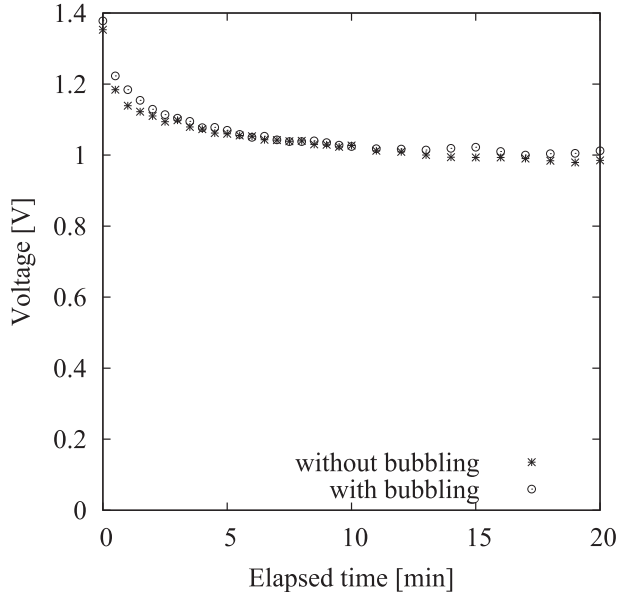

Fig. 8. Effect of bubbling on constant current discharge curves at 20 mA^{-2} cm^{-2} and $W_{C/carbonate}$ = 3.0 wt%.

$$C + CO_3^{2-} \rightarrow 2CO + O^{2-} \quad \text{(R15)}$$

Electrochemical reaction mechanisms after O^{2-} formation are summarized in previous studies [5,29]. Briefly, they are as follows.

First, O^{2-} adsorbs on the reactive carbon surface (C_{RS}), and forms a strongly bound CO functional group at reactive carbon sites ($C_{RS}O$).

O^{2-} adsorption on the reactive carbon surface and electron discharge:

$$C_{RS} + O^{2-} \rightarrow C_{RS}O + 2e^- \quad \text{(R16)}$$

Then, O^{2-} adsorbs at $-C_{RS}O$ sites, and CO_2 is produced electrochemically (R17 and R18). If the $C_{RS}O$ is desorbed before the adsorption of the second O^{2-}, then CO is produced (via R19) [29]. This group decomposes very slowly to form CO (R19) [17].

O^{2-} adsorption at $C_{RS}O$ sites (RDS):

$$C_{RS}O + O^{2-} \rightarrow C_{RS}O_2^{2-} \quad \text{(R17)}$$

CO_2 desorption and electron discharge:

$$C_{RS}O_2^{2-} \rightarrow CO_2 + 2e^- \quad \text{(R18)}$$

CO desorption (partial electrochemical oxidation):

$$C_{RS}O \rightarrow CO\,(g) \quad \text{(R19)}$$

The C/O^{2-} ratio is a key to inhibit partial electrochemical oxidation. As noted previously, bubbling provides both C and O^{2-} ions to the Au surface by stirring, and it removes a small amount of gas from the carbon/carbonate slurry. When the C/O^{2-} ratio is low, as at $W_{C/carbonate}$ = 1.0 wt%, complete electrochemical oxidation (R16 through R18) becomes dominant, and Ar bubbling inhibits partial electrochemical oxidation (R19), as shown in Fig. 9. This is because O^{2-} ion transport is dominant. However, when the C/O^{2-} ratio is high, as at $W_{C/carbonate}$ = 3.0 wt%, partial electrochemical oxidation (R19) becomes dominant, as shown in Fig. 10. The bubbling effect becomes insignificant, because carbon transport is more dominant, and the amount of CO that forms is beyond the capacity of Ar bubbling. Therefore, the impact of bubbling is dictated by the C/O^{2-} ratio.

Combining the above elemental steps, global anode reactions (R1, R4, and R5) can be derived. R1 is derived from R14, R16, R17, and R18. R4 is derived from R14, R16, and R19. R5 is derived from R15, R16, and R19. These pathways are described in Fig. 11.

Many researchers have proposed equations to evaluate the DCFC performance. In some literature, carbon efficiency is calculated on the basis of the assumption that carbon is consumed through R1 and R6 (the Boudouard reaction) [4,13,14]. However, in this study, CO is mainly produced from partial electrochemical oxidation. Therefore, in this study, it is appropriate to use coulombic efficiency (η_c), which is defined as the ratio of integrated cell current to the current calculated for 4-electron transfer per atom of carbon [15]. Cooper and Selman suggested a formula to calculate coulombic efficiency (Eq. (6)) on the basis of R1 and R4 [15,16]:

$$\eta_c = \frac{a+2}{2(2a+1)} \quad (6)$$

where a is the ratio of CO_2 and CO production rate.

Our results show that CO/CO_2 ratio is quite higher than unity at $W_{C/carbonate}$ = 3.0 wt%. However, maximum CO/CO_2 ratio is unity when R1 and R4 are used. To explain high CO production rate, R5 that produces only CO during discharge is necessary.

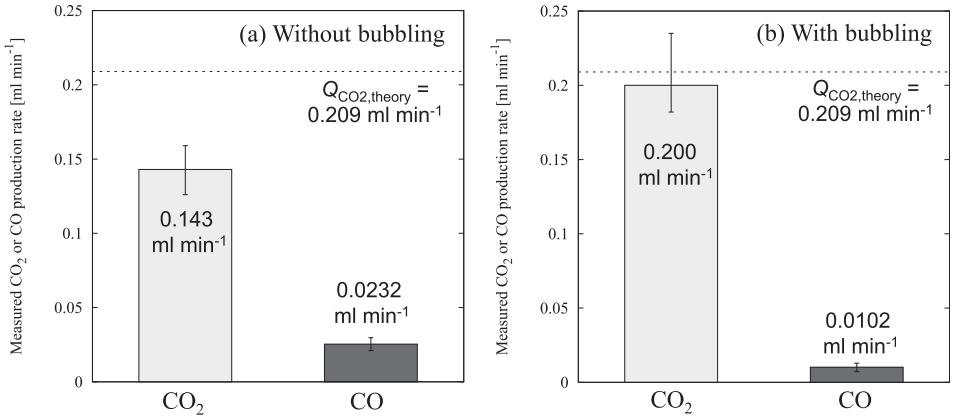

Fig. 9. Effect of bubbling on measured CO_2 and CO production rate during discharge at 20 mA cm^{-2} (at $W_{C/carbonate}$ = 1.0 wt%).

Thus, in this research, R1 and R5 were used to calculate coulombic efficiency. When the equation of coulombic efficiency is derived, the following reactions (R20 and R21) are useful.

$$xC + 2xCO_3^{2-} \rightarrow 3xCO_2 + 4xe^- \quad \text{(R20)}$$

$$yC + (1/2)yCO_3^{2-} \rightarrow (3/2)yCO + ye^- \quad \text{(R21)}$$

where x and y indicate carbon consumption ratios for R1, and R5, respectively. The sum of x and y is given as follows:

$$x + y = 1 \quad (7)$$

Coulombic efficiency (η_c) is defined as $n/4$, where n is the equivalent charge associated with electrochemical oxidation of one mole of carbon. η_c, $Q_{CO2,x,y}$, and $Q_{CO,x,y}$ are derived as follows:

$$\eta_c = \frac{n}{4} = \frac{(4x+y)}{4} \quad (8)$$

$$Q_{CO_2,\text{product},x,y} = \frac{(3x)IV_m}{(4x+y)F} \quad (9)$$

$$Q_{CO,\text{product},x,y} = \frac{(3y/2)IV_m}{(4x+y)F} \quad (10)$$

In this approach, the number of unknown coefficients is two (x and y). The number of independent equations is also two (Eqs. (9) and (10)). No other unknown coefficients can be added. The formula of coulombic efficiency (Eq. (8)) can be rewritten to be function of the ratio of CO_2 and CO (a) as follows:

$$\eta_c = \frac{(4x+y)}{4} = \frac{(4x+y)}{4(x+y)} = \frac{\left\{2+\left(\frac{y}{2x}\right)\right\}}{2\left\{1+2\left(\frac{y}{2x}\right)\right\}} = \frac{a+2}{2(2a+1)} \quad (11)$$

When Eq. (11) is derived, $x + y = 1$ (Eq. (7)) is used. Eq. (11), derived from R1 and R5, is the same as Eq. (6), which is derived from R1 and R4. This is because R5 can be derived from R1 and R4 by eliminating CO_2 mathematically. R1 and R5 can be used when the CO/CO_2 ratio is larger than unity. Q_{CO2} and Q_{CO} are also a function of a, as shown by the following:

$$Q_{CO_2,a,\text{product}} = \frac{3IV_m}{2(2+a)F} \quad (12)$$

$$Q_{CO,a,\text{product}} = \frac{3aIV_m}{2(2+a)F} \quad (13)$$

On the basis of Eqs. (11) through (13), η_c, $Q_{CO2,a,\text{product}}$ and $Q_{CO,a,\text{product}}$ can be determined from the measured CO/CO_2 ratio (=a). This approach is defined as "a function" in this study.

In addition to Eq. (11), coulombic efficiency can be determined from Eq. (8) by minimizing the error term defined as the followings:

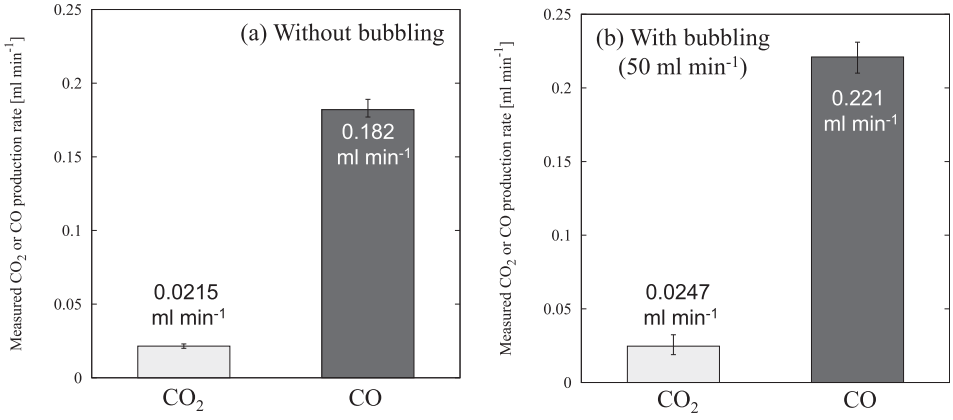

Fig. 10. Effect of bubbling on measured CO_2 and CO production rate during discharge at 20 mA cm^{-2} (at $W_{C/carbonate}$ = 3.0 wt%).

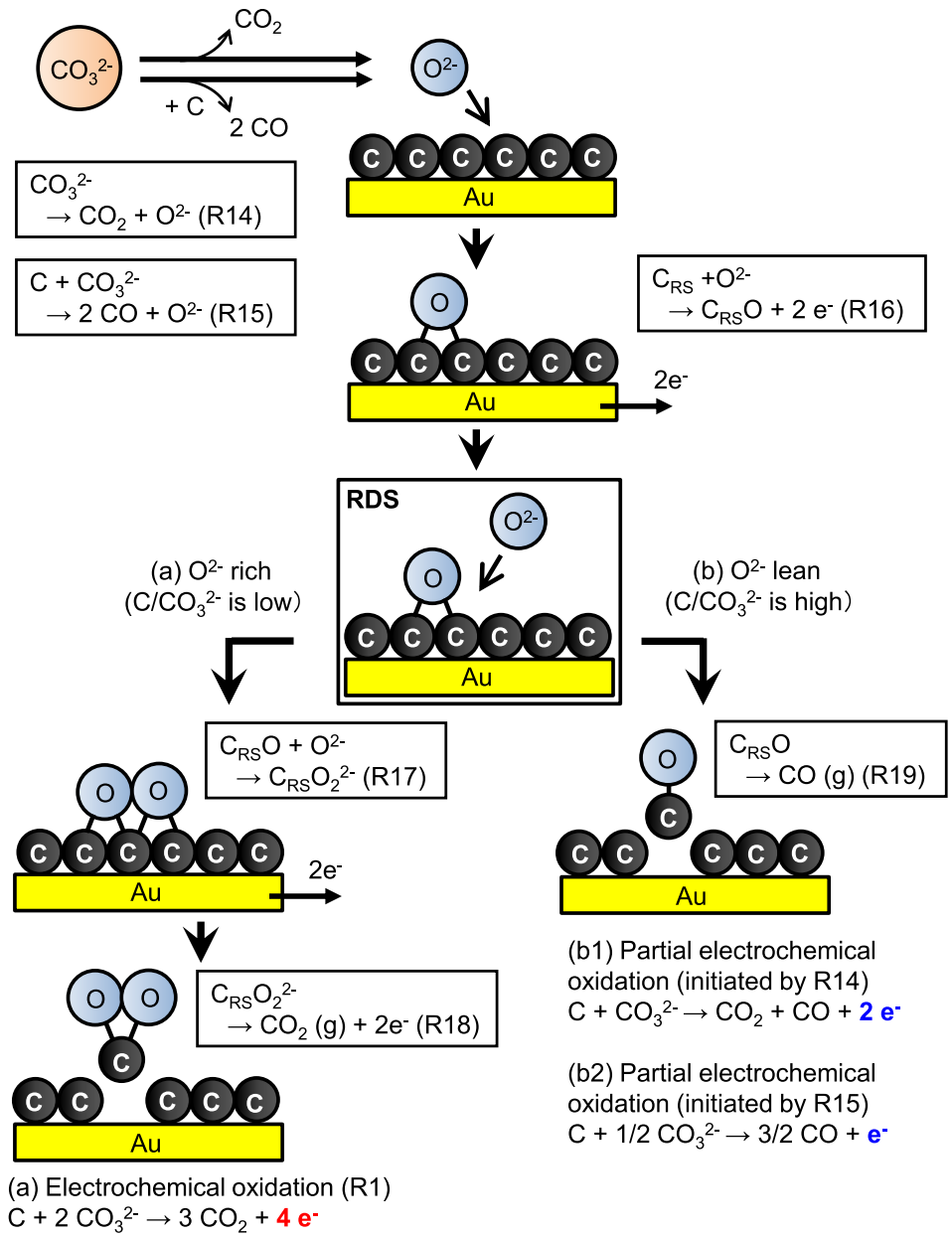

Fig. 11. Reaction mechanisms for electrochemical oxidation of carbon in molten carbonate (partially referring [3]).

$$\varepsilon_{CO_2+CO} = \frac{\left|Q_{CO_2,product,exp} - Q_{CO_2,x,y,product}\right|}{Q_{CO_2,product,exp}} + \frac{\left|Q_{CO,product,exp} - Q_{CO,x,y,product}\right|}{Q_{CO,product,exp}} \quad (14)$$

In this approach, carbon consumption ratios (x and y) that provide minimum error term are determined by x-sweeping, which is similar to the least square method. Then, Q_{CO2}, Q_{CO}, and η_c are determined by Eqs. (8) through (10). This approach is defined as "min. error" in this study.

Fig. 12 shows measured and calculated CO and CO_2 production rates at $W_{C/carbonate} = 1.0$ wt%. Without bubbling, the measured CO_2 production rate is lower than the calculated values (Fig. 12(a)). However, the difference is not so significant, this difference might be because of unknown factors in partial electrochemical oxidation of activated carbon. Another possible explanation is that, Li_2O and CO_2 undergo a recombination reaction, given as R22 which leads to a lower CO_2 production rate.

$$Li_2O + CO_2 \rightarrow Li_2CO_3 \quad (R22)$$

Meanwhile, bubbling inhibits partial electrochemical oxidation, leading to low CO formation (Fig. 12 (b)). Table 3 shows estimated coulombic efficiencies and error terms. Ar bubbling improves coulombic efficiencies by about 10%, regardless of approach ("a function" or "min. error").

Fig. 13 shows measured and calculated CO and CO_2 production rates at $W_{C/Carbonate} = 3.0$ wt%. Contrary to the case at $W_{C/carbonate} = 1.0$ wt%, calculated CO production rate is 50% higher than the experimental rate. This suggests that the detected CO and CO_2 production rates are insufficient for discharge at 20 mA cm^{-2}, indicating products other than CO and CO_2 form during discharge. R12, in which the product is Li_2CO_3, may explain this difference. If R12 is processed, gas products are reduced, while current is kept

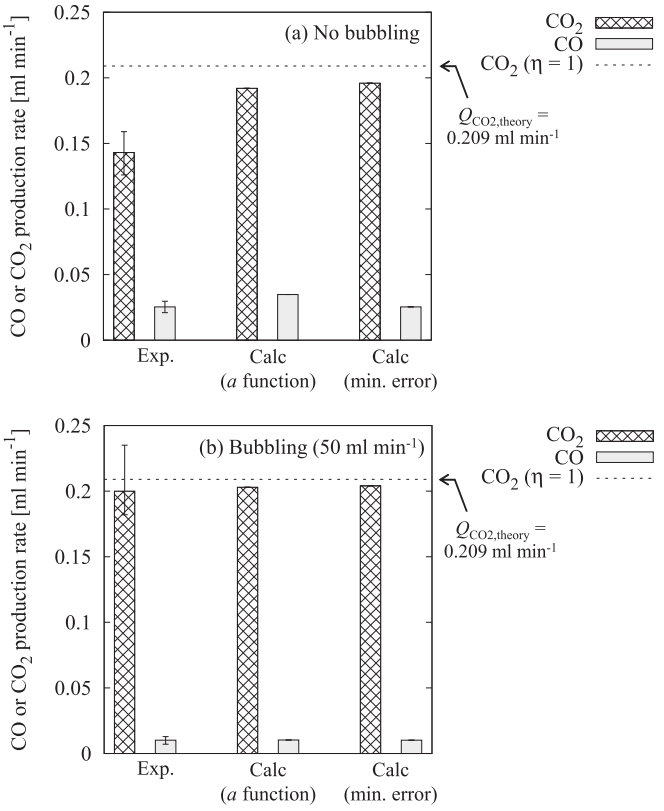

Fig. 12. Experimental and calculated CO and CO_2 production rate (W_C/carbonate = 1.0 wt%).

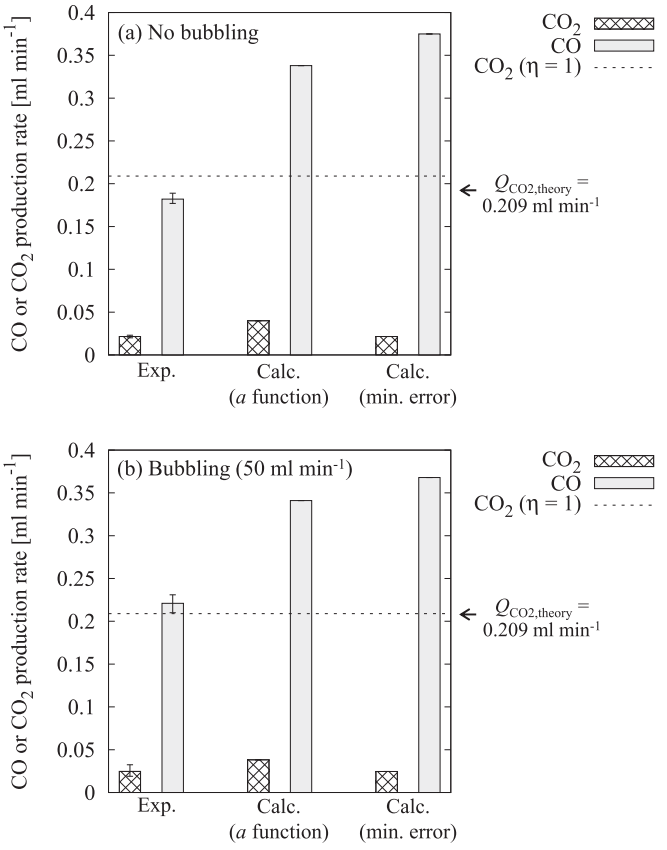

Fig. 13. Experimental and calculated CO and CO_2 production rate (W_C/carbonate = 3.0 wt%).

constant. This provides additional evidence that R12 is processed during discharge and at higher OCVs of 1.3–1.4 V. It also indicates that coulombic efficiency cannot be determined from R1 and R5 at $W_{C/carbonate}$ = 3.0 wt%. Therefore, another formula is necessary to estimate coulombic efficiency in this case.

Table 4 shows coulombic efficiency (η_c), voltage efficiency (η_{vol}) and total electrochemical efficiency (η_{total}) of the DCFC at $W_{C/carbonate}$ = 1.0 wt%. Total electrochemical efficiency is determined by the following equations.

$$\eta_{total} = \frac{n\mathrm{F}\Delta E}{\Delta H} = \frac{n}{n_{theory}} \times \frac{\Delta E}{\left(\Delta G^0 \Big/ n_{theory}\mathrm{F}\right)} \times \frac{\Delta G^0}{\Delta H^0} \left(= \eta_c \times \eta_{vol} \times \eta_{theory} \right) \quad (15)$$

where carbon (graphite) data is used as the theoretical value, n_{theory} is 4 and ΔE is cell voltage. The "error min." approach is used to calculate coulombic efficiency. Voltage efficiency is determined from the current discharge curve at the steady state, as shown in Fig. 7. Bubbling increases the total efficiency of the DCFC from 52 % to 64 %.

Table 3
Coulombic efficiency of the DCFC at $W_{C/carbonate}$ = 1.0 wt%.

	Without bubbling		With bubbling	
	a function	Min. error	*a* function	Min. error
η_c [−]	0.82	0.86	0.93	0.93
ε_{CO2+CO} [%]	70	38	3.7	1.9

4. Conclusion

This study aims to enhance DCFC efficiency by bubbling Ar gas in a carbon/carbonate slurry. The DCFC developed here, which is of a cartridge type, used a porous alumina tube to contain carbon/carbonate slurry as fuel. The DCFC was operated at 1073 K, and current discharge curve and CO and CO_2 production rates were measured during discharge at 20 mA cm^{-2}. When the carbon content in carbonates ($W_{C/carbonate}$) was 1.0 wt%, Ar bubbling decreased the CO/CO_2 production ratio from 0.16 to 0.051, and increased the CO_2 production rate, which approached the theoretical value for complete electrochemical oxidation of carbon. From the balance of these production rates, CO was mainly formed from partial electrochemical oxidation rather than the Boudouard reaction. It was shown that bubbling inhibited partial electrochemical oxidations. Moreover, bubbling increased the cell voltage by approximately 0.1 V at steady state. At $W_{C/carbonate}$ = 3.0 wt%, the CO/CO_2 production ratio without bubbling increased significantly to 8.5, indicating that partial electrochemical oxidation was dominant. The amount of CO formed at $W_{C/carbonate}$ = 3.0 wt% was sufficient for CO and/or the alkali ions to intervene in the discharge process, which showed a higher OCV (=1.3 V).

Table 4
Coulombic, voltage, and total efficiencies of DCFC at $W_{C/carbonate}$ = 1.0 wt%.

	With bubbling	Without bubbling
η_c (min. error) [−]	0.93	0.86
η_{vol} [−]	0.69	0.60
η_{total} [−]	0.64	0.52

Therefore, voltage at $W_{C/carbonate}$ = 3.0 wt% was higher than that at $W_{C/carbonate}$ = 1.0 wt%. At $W_{C/carbonate}$ = 3.0 wt%, bubbling did not influence the current discharge curve, whereas it did at $W_{C/carbonate}$ = 1.0 wt%. Considering reaction pathways, the C/O^{2-} ratio was a key to explain the electrochemical oxidation of carbon. When the C/O^{2-} ratio was low like, as at $W_{C/carbonate}$ = 1.0 wt%, complete electrochemical oxidation became dominant, and bubbling enhanced complete electrochemical oxidation by stirring. However, when the C/O^{2-} ratio was high, as at $W_{C/carbonate}$ = 3.0 wt%, partial electrochemical oxidation became dominant, and bubbling did not inhibit partial electrochemical oxidation because carbon transport became dominant. Bubbling provided both C and O^{2-} ions to the Au surface by stirring. However, the impact of bubbling was dictated by the C/O^{2-} ratio. Bubbling also promoted removal of gases from the carbon/carbonate slurry. When $W_{C/carbonate}$ = 1.0 wt%, bubbling increased both coulombic and voltage efficiencies, resulting in an increase in total efficiency from 52% to 64%.

Acknowledgment

This study was partly supported by a JSPS Grant-in-Aid for challenging Exploratory Research (No. 25630064), and J-Power.

Nomenclature

a	the ratio of CO_2 and CO production rate [−]
d_{002}	interplanar distance [nm]
E_0	standard potential [V]
F	Faraday constant [C mol^{-1}]
I	current flow [A] (=C s^{-1})
I_d	current flow density [A cm^{-2}]
L_a	the layer dimension parallel to the basal plane [nm]
L_c	the layer dimension perpendicular to the basal plane [nm]
M	metal indicating K, Na or Li
n	equivalent charge associated with electrochemical oxidation of one mole of carbon [−]
Q_i	flow rate of species i (i = CO or CO_2) [ml min^{-1}]
$Q_{CO2,theory}$	theoretical CO_2 production rate for complete electrochemical oxidation of carbon at 20 mA [ml min^{-1}]
$Q_{i,product}$	gas production rate of species i during discharge [ml min^{-1}]
$Q_{i,x,y,product}$	calculated gas production ratio of species i determined by x and y [ml min^{-1}]
$Q_{i,a,product}$	calculated gas production ratio of species i determined by a [ml min^{-1}]
V_m	molar volume of CO_2 [ml mol^{-1}]
$W_{C/carbonate}$	carbon content in the carbonates [wt%]
X_i	mole fraction of species i (i = CO or CO_2) [ml min^{-1}]
x, y	carbon consumption ratios for R1 and R5 [−]

Greek symbol

ε_{CO2+CO}	error term in Eq. (14) [−]
η	coulombic efficiency [−]
ΔE	cell voltage [V]
ΔG^0	Gibbs free energy [kJ mol^{-1}]
ΔH^0	enthalpy [kJ mol^{-1}]

Subscript

c	coulombic
exp	experiment
vol	voltage

References

[1] S. Giddey, S.P.S. Badwal, A. Kulkarni, C. Munnings, Prog. Energy Combust. Sci. 38 (2012) 360–399.
[2] A.L. Dicks, J. Power Source 156 (2006) 128–141.
[3] A.C. Rady, S. Giddey, S.P.S. Badwal, B.P. Ladewig, S. Bhattacharya, Energy Fuels 26 (2012) 1471–1488.
[4] D.G. Vutetakis, D.R. Skidmore, H.J. Byker, J. Electrochem. Soc. 134 (1987) 3027–3035.
[5] N.J. Cherepy, R. Krueger, K.J. Fiet, A.K. Jankowski, J.F. Cooper, J. Electrochem. Soc. 152 (2005) A80–A87.
[6] X. Li, Z.H. Zhu, R.D. Marco, A. Dicks, J. Bradley, S. Liu, et al., Ind. Eng. Chem. Res. 47 (2008) 9670–9677.
[7] C.G. Lee, H. Hur, M.B. Song, J. Electrochem. Soc. 158 (2011) B410–B415.
[8] G.A. Hackett, J.W. Zondlo, R.J. Svensson, J. Power Source 168 (2007) 111–118.
[9] M. Ihara, S. Hasegawa, J. Electrochem. Soc. 153 (2006) A1544–A1546.
[10] S. Hasegawa, M. Ihara, J. Electrochem. Soc. 155 (2008) B58–B63.
[11] T.M. Gür, J. Electrochem. Soc. 157 (2010) B751–B759.
[12] X. Li, Z. Zhu, R.D. Marco, J. Bradley, A. Dicks, J. Phys. Chem. A 114 (2010) 3855–3862.
[13] Q. Liu, Tian Ye, Xia Chun, L.T. Thompson, B. Liang, Y. Li, J. Power Source 185 (2008) 1022–1029.
[14] X. Li, Z. Zhu, R.D. Marco, J. Bradley, A. Dicks, J. Power Source 195 (2010) 4051–4058.
[15] J.F. Cooper, J.R. Selman, Int. J. Hydrog. Energy 37 (2012) 19319–19328.
[16] J.F. Cooper, J.R. Selman, Electrochem. Soc. Trans. 19 (15) (2009).
[17] C.Q. Wang, J. Liu, J. Zeng, J.L. Yin, G.L. Wang, D.X. Cao, J. Power Sources 233 (2013) 244–251.
[18] D.W. McKee, Fuel 62 (1983) 170–175.
[19] S.J. Yuh, E.E. Wolf, Fuel 63 (1984) 1604–1609.
[20] J.W. Kim, H.G. Lee, Metallurgical Mater. Trans. B 32B (2001) 17–24.
[21] NIST–JANAF Thermochemical Tables, http://kinetics.nist.gov/janaf/.
[22] H. Li, Q. Liu, Y. Li, Electrochimica Acta 55 (2010) 1958–1965.
[23] D. Cao, Y. Sun, G. Wang, J. Power Source 167 (2007) 250–257.
[24] T.M. Gür, Chem. Rev. 113 (2013) 6179–6206.
[25] Y. Nabae, K.D. Pointon, J.T.S. Irvine, Energy Environ. Sci. 1 (2008) 148–155.
[26] Y. Nabae, K.D. Pointon, J.T.S. Irvine, J. Electrochem. Soc. 156 (2009) B716–B720.
[27] K. Nagase, T. Shimodaira, M. Itoh, Y. Zheng, Phys. Chem. Chem. Phys. 1 (1999) 5659–5664.
[28] A. Elleuch, J. Yu, A. Boussetta, K. Halouani, Y. Li, Int. J. Hydrogen Energy 38 (2013) 8514–8523.
[29] C. Li, Y. Shi, N. Cai, J. Power Sources 196 (2011) 754–763.